Characterization and modelling of air humidification in Fuel Cell System for transport sector

Amedeo Grimaldi[1,*], *Lorenzo* Villa[1], *Andrea* Baricci[1], *Stefano* De Antonellis[1], *Claudio* Oldani[2], and *Andrea* Casalegno[1]

[1]Politecnico di Milano, Energy Department, 20156 Milano, Italy
[2]Solvay Specialty Polymers SpA, R&D Centre, 20021 Bollate, Italy

Abstract. A model for the physical description of water transport through steady-state permeation and dynamic sorption within perfluoro-sulfonic acid (PFSA) membranes has been developed. A broad experimental campaign is conducted on several membranes, belonging to Aquivion class, varying both in thickness and equivalent weight (EW). The experimental data have been used to calibrate and validate water transport model and to find correlations for mass-transfer properties in low-EW PFSA membranes that describe consistently both water vapor permeation and sorption. It has been possible to identify individual contributions to mass transport resistance and to determine the optimal configuration and materials of a full-scale counter-flow membrane humidifier under a set of specific operating conditions.

1 Introduction

High durability and efficiency in state-of-the-art polymer electrolyte membrane (PEM) fuel cells are strongly dependent on membrane hydration state and external humidification of the reactant streams is essential [1]. Passive humidification techniques seem to be the most viable solution for automotive applications and could be developed using PFSA membranes, already adopted as electrolyte in PEM fuel cells where water management is a crucial phenomenon for efficient operation.

Water uptake features of PFSA ionomers have been investigated over the past few decades and water diffusion and sorption properties through membranes are generally determined using experimental methods, such as dynamic water sorption (DVS), steady state diffusion or permeability, pulsed-field gradient spin-echo (PGSE) nuclear magnetic resonance (NMR), and time-resolved Fourier transform infrared-attenuated total reflectance (FTIR) spectroscopy [2]. A complete understanding of mechanisms underlying water transport through PFSA ionomer is still under investigation. Water diffusivity values reported in literature vary up to four orders of magnitude, i.e. 10^{-14} to 10^{-9} m^2/s, depending on the experimental method [2].

In the following, starting from a batch of short-side chain PFSA membranes, belonging to Aquivion class, a transport model is developed, able to simulate two different experimental techniques, especially water permeation and DVS tests.

A unique formulation for water transport properties, independent of the experimental method is obtained. Performances and size of a full-scale automotive PEM fuel-cell humidifier under real operative conditions are estimated.

2 Experimental Setup

Prior to testing, all membrane samples have undergone a standard cleaning procedure, consisting in regenerating each sample by boiling it for 30 minutes in deionized water and letting it dry for 12 hours into a beaker before testing.

Permeation testing aims at obtaining steady-state data of the water permeation rate through the membrane-gas diffusion layer (GDL) assembly. Membrane area, A_{cell}, is equal to 8 cm^2. Dry air flow rate values on dry side, $\dot{V}_{air}^{dry}$, are 0.5, 1.0 and 1.5 SLPM, that correspond to the typical flow rates on humidifier and are scaled on membrane area. Dry air flow rate on wet side is 2 SLPM, before entering in a bubbler and getting humidified with a given dew point temperature, that is varied to test different inlet RH for wet stream. Gas flow rate values on dry side are chosen smaller than the wet-side ones to avoid very low dry-side RH conditions at the outlet. Air is fed in a co-flow configuration. The cell temperature values are chosen to match the typical operative conditions of a PEM fuel cell, from start-up to full power.

The permeated water flux rate, $\dot{m}$, is computed through Equation (1), assuming that dry air behaves as a perfect gas and that its permeation rate through the membrane is negligible.

$$\dot{m} = \frac{MM_{H_2O}}{A_{cell}} \frac{\frac{RH_{out}^{dry}}{100}}{\frac{p_{out}}{p_{H_2O}^{sat}\left(T_{out}^{dry}\right)} - \frac{RH_{out}^{dry}}{100}} \frac{\dot{V}_{air}^{dry}}{22.414} \quad (1)$$

where RH_{out}^{dry}, p_{out}, T_{out}^{dry} are RH, pressure and temperature of the stream on dry side outlet.

* Corresponding author: amedeo.grimaldi@polimi.it

Absorption tests have been carried out using an automated, gravimetric, dynamic water sorption analyzer, namely AQUADYNE DVS™ 2 produced by Quantachrome Instruments. Each membrane sample is conditioned as described above, before being tested, and is placed over a balance plate of the gravimetric analyzer.

The overall dry gas fed to the machine throughout the test is kept constant at 100 Standard Cubic Centimeters per minute (SCCM). Once the drying step is completed at 80°C in a nitrogen atmosphere at ambient pressure, to obtain the reference dry mass, m_{dry}, the samples are subject to increasing-humidity conditions within the range 0% to 90% RH, with 5% intervals, at a given temperature.

The DVS instrument measures mass change over time for samples and automatically switches to the following step when the cut-off condition is reached. Tests are performed at different temperatures, 30, 50, 70 °C respectively.

The membrane water content λ is computed for each sample by knowing the dynamic mass measurement, $m(t)$, the mass of the dry ionomer, m_{dry}, and the sample's equivalent weight.

$$\lambda(t) = \frac{m(t) - m_{dry}}{m_{dry}} \frac{EW}{M_{H_2O}} \tag{2}$$

From the absorption curves over time, it is possible to distinguish a two-step process with two rate constants largely separated in time, as reported in [2],[3]. The first mechanism is generally related to mass transport resistances, mainly external gas convection and interfacial membrane resistance, and predominates at short time. The latter mechanism takes over at longer times, suggesting that water uptake becomes controlled by the polymer rearrangement and relaxation.

3 Model Formulation

3.1. Model Domain

For the water permeation test setup, framework consists of five regions that represent wet and dry gas channel, wet and dry porous media, and ionomer, similar to configuration in a typical plate and frame humidifier. For the DVS test setup, ionomer is exposed to humidified air on both sides, thus determining the presence of the external convection together with water uptake and diffusion through ionomer.

It has been assumed that transport model is isothermal since tests are performed at constant temperature; moreover, water diffusion is assumed to occur only through ionomer thickness, whereas planar diffusion is assumed to be negligible; single phase is modelled for water in porous media.

In the following, first, the governing equations for each domain will be presented, then permeation and sorption models' framework are described.

3.2 Model Equations

Generally, water transport through ionomer is described in terms of λ, that indicates the moles of water molecules per moles of sulfonic acid group, thanks to equation (3), where D_λ is the effective diffusion coefficient of water through ionomer, proportional to the hydration state of membrane.

$$\frac{\partial \lambda}{\partial t} = \nabla \cdot (D_\lambda \nabla \lambda) \tag{3}$$

$$\dot{N}_w^{int} = k_{ad} \frac{\rho_i}{EW} (\lambda^* - \lambda) \tag{4}$$

$$\lambda^* = (1 - \phi)\lambda^{eq} + s_{relax} \tag{5}$$

$$\frac{\partial s_{relax}}{\partial t} = -\frac{1}{\tau_{relax}} (s_{relax} - \phi \lambda_{eq}) \tag{6}$$

Water sorption and desorption, occurring at membrane interfaces, can be modelled by equation (4), where k_{ad} is the interfacial water transfer coefficient, assumed to be function of λ, and λ^*, described by equation (5), is the quasi-equilibrium value for water content in the ionomer, as a consequence of transient swelling of polymer backbone of ionomer [3].

Relaxation model, described in [4], has been implemented. Indeed, the quasi-equilibrium value for water content, λ^*, is obtained according to equation (6), where ϕ represents the further volume for water accumulation that becomes available as polymer relaxes over time and s_{relax} accounts for the dynamics of stress relaxation, that is assumed to be described by a first-order dynamics, as observed by Satterfield et al.[5].

Stress relaxation factor ϕ ranges between 0.15 and 0.3 whereas the relaxation time constant, τ_{relax}, is assumed to be 3500 s, close to findings in [5]. The equilibrium water content, λ_{eq}, is function of water activity and temperature and adsorption isotherms are obtained from DVS experiments.

Gas diffusion trough porous medium, adjacent to gas channels, is governed by the following equation.

$$\nabla \cdot \left(D_i^{eff} \nabla c_i \right) = 0 \tag{7}$$

$$D_i^{eff} = \varepsilon \left(\frac{\varepsilon - \varepsilon_{pc}}{1 - \varepsilon_{pc}} \right)^{n_e} \frac{1 - y_i}{\sum_{j \neq i}^{N_{species}} \frac{y_j}{D_{ij}}} \tag{8}$$

Where ε is the compressed layer porosity, c_i denotes the concentration of species i, D_i^{eff} is the effective diffusivity of species i which is calculated by accounting for molecular diffusion and for the tortuous pathway through porous layers.

In Equation (8), ε_{pc} is the percolation threshold, assumed to be 0.11 [6].

Conservation equations for mass, inside channel volumes, are solved for each species along channel direction.

$$\nabla \cdot \dot{N}_i = \frac{\dot{N}_i^{\mathrm{GDL|CH}}}{L_{ch}} \tag{9}$$

$$\nabla p = -\frac{f \mu}{2 \, d_h^2} \frac{\dot{N}}{\frac{h_{ch}}{L_{ch}} \frac{p}{R \, T}} \tag{10}$$

where c_i, $\dot{N}_i$, $\dot{N}_i^{\mathrm{GDL|CH}}$ are the molar concentration, molar fluxes along channel direction and molar fluxes at GDL/channel interface of species i, whereas $\dot{N}$ and p are the local total molar flux and pressure in gas channels. f is the friction factor evaluated according to Pant et al. [7].

$$\dot{N}_i^{\mathrm{GDL|CH}} = h_m(c_i - c_i^{GDL|CH}) \qquad (11)$$

In the case of flow inside a channel, as in the first setup, h_m is dependent upon Sherwood number, that is related to local operating conditions.

For the second setup, where humidified air is flowing externally over the ionomer sample, h_m is estimated from literature, equal to 2×10^{-3} m/s [8]. All the other gas properties are taken from literature.

The transport model has been implemented in MATLAB, and, according to the frameworks, shown above, two different versions of the transport model have been implemented. In particular, a steady-state model is used for simulating water permeation tests, whereas a transient model for the water uptake.

4 Results and Discussion

In Figure 1-2-3, water flux is plotted against mean logarithmic water vapor concentration difference, $\Delta C_{ml} = (\Delta C_{in} - \Delta C_{out})/ln\,(\Delta C_{in}/\Delta C_{out})$ that represents the driving force of the process. ΔC_{in} and ΔC_{out} denote the difference between water vapor concentration of the inlet and the outlet streams, respectively.

Focusing on membrane properties, in Figure 1(a), it is possible to observe the effect of thickness on water transport, for membranes with same *EW*, i.e. 980 g mol^{-1}. As expected, by increasing membrane thickness, water flux is lower, since diffusion through membrane is hindered. It is noticeable that, as thickness increases by three times, maximum water flux at 80°C is twofold. As visible in Figure 1(b), water sorption over time results to be affected as well. In particular, higher thickness slows down water uptake in the first step, dominated by mass transport resistance. In the second regime, dominated by ionomer relaxation, no visible effect can be noted, thus suggesting that ionomer relaxation is independent upon thickness.

In Figure 2(a), it is shown the global water flux for membranes with same thickness, i.e. 50 μm and different *EW*, for three values of membrane temperature. It can be noted that, by decreasing *EW*, water flux gets higher. As ΔC_{ml}increases, water flux increases as well, since inlet RH of wet stream is increasing. At the same time, looking at water absorption curves, in Figure 2(b), it results that water uptake is slightly faster for membrane with lower *EW*. A slight deviation among the curves is visible as well in the second regime, indicating that ionomer relaxation is faster for lower *EW*.

Effect of porous layer treatment has been analyzed and it has enlightened that using hydrophilic porous layer on both wet and dry side allows to have a higher water flux,

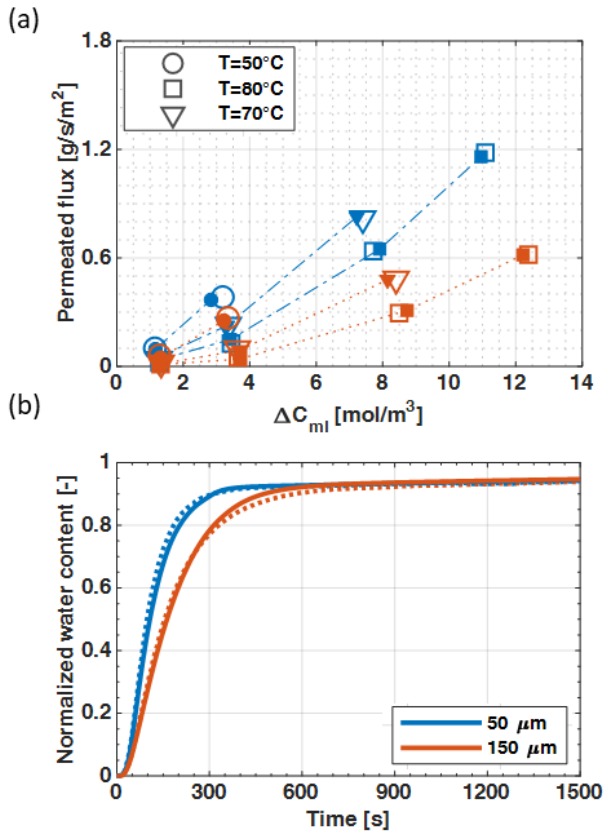

Fig. 1 Effect of membrane thickness: (a) Water permeation flux; (b) Water sorption over time. (Experimental data: void symbols in (a) and dashed lines in (b); Model simulations: solid symbols in (a) and solid lined in (b))

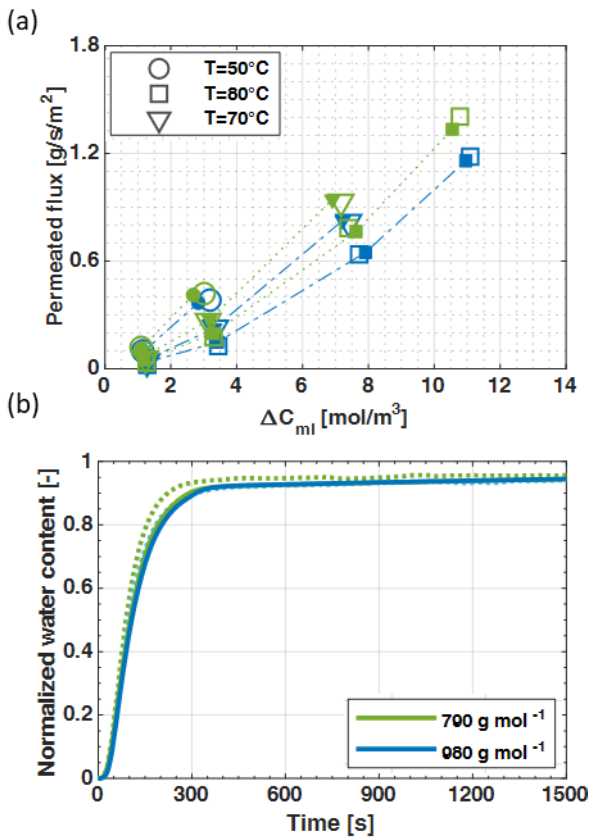

Figure 2 Effect of membrane *EW*: (a) Water permeation flux; (b) Water sorption over time. (Experimental data: void symbols in (a) and dashed lines in (b); Model simulations: solid symbols in (a) and solid lined in (b))

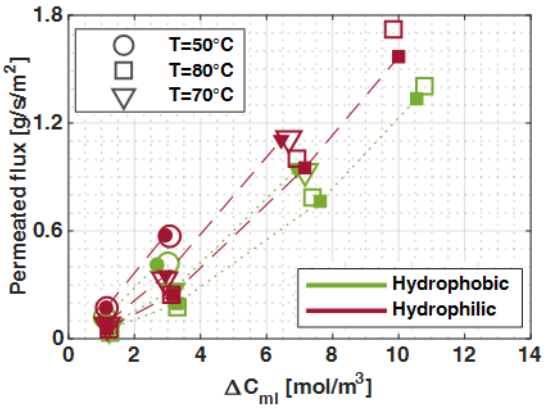

Fig. 4 Effect of porous layer treatment: Water permeation flux. (Experimental data: void symbols; Model simulations: solid symbols)

with respect to having hydrophobic one on both sides or mixed configuration with hydrophilic on dry side and hydrophobic on wet side, under every operating conditions. It is beneficial, also, to reduce thickness of the layer, thus, to reduce its mass transport resistance. Moreover, it has been observed, by overlapping several layers of porous layers, that effective vapor diffusivity through the layer itself is independent of the treatment, indicating that decrease in mass transport resistance is ascribable to diminishing of the other contributions.

Correlations for D_λ and k_{ad} are reported, obtained by fitting of the experimental data, shown in Figure 1 and 2, implemented according to Paragraph 2, exploiting the functional forms proposed by Kulikovsky [9] for D_λ and Ge et al. [10] for k_{ad}:

$$D_\lambda = \left(\frac{\lambda}{25}\right)^{0.15} [1 + tanh(\lambda - 2.1g^{0.5})] \\ 4.22 \times 10^{-10}\, g^{0.66} exp\left[\frac{15000}{R}\left(\frac{1}{343} - \frac{1}{T}\right)\right] \quad (12)$$

$$k_{ad} = 10.1 \times 10^{-5} f_v \exp\left[\frac{40000}{R}\left(\frac{1}{343} - \frac{1}{T}\right)\right] \\ \text{with} \quad f_v = \frac{1.8\times10^{-5}\,\lambda}{\frac{EW}{\rho_i} + 1.8\times10^{-5}\,\lambda} \quad (13)$$

where $g = EW/980$ accounts for the effect of EW on diffusion coefficient. For low water content, diffusion coefficient D_λ results to be slightly higher for lower EW, whereas, as λ increases, it tends to a lower maximum value. This feature could be maybe attributed to an increase in tortuosity of water channel domains, whose effect is incorporated in D_λ[2].

Table 1 DOE reference condition and geometrical dimensions of humidifier cell

Parameter	Dry Air	Wet Air
$\dot{V}_{air}^{dry}[SLPM]$	3000	2600
T [°C]	80	80
P [$mbar$]	1830	1600
RH [%]	0%	85%
$A_{cell}[cm^2]$	100	
Channel height/width [mm]	0.85/0.85	

Actually, it has been observed that, as EW decreases, width of hydrophilic channels decrease in size and water cluster distribution becomes more dispersed inside membrane volume, determining a tortuous path for water transport, especially at higher degrees of hydration [11].

On the other side, local water concentration increases, as a consequence of an increase in density of sulfonic acid groups, determining a higher water flux for membranes with lower EW membranes, with the same driving force ΔC_{ml}.

The interfacial constant, k_{ad}, considering the formulation of Ge et al. [10] is affected as well by EW, since it is related to water volume fraction, f_v, that increases as EW decreases, for the same value of water content λ.

The greater performance, associated to hydrophilic porous layer can be incorporated in the model, assuming that interfacial adsorption/desorption becomes very fast for high ΔC_{ml}, thus meaning a negligible contribution by interfacial transport resistance. It is possible to relate this aspect to the likely presence of liquid film on the membrane interfaces, whose growth is favored by hydrophilicity of the porous layer, that would determine a strong decrease in the interfacial surface resistance, as also reported in Weber et al. [2].

Validation of transport model has been performed thanks to water uptake curves from DVS analyzer.

Model simulations are well adherent to experimental data, mainly for low and medium values of RH. For higher RH, a slower uptake is generally visible, and it has been noted that a limiting factor is the slower dynamics of average RH in the weighting chamber, that is affected by a greater accumulation of water inside the ionomer. The slower uptake is consistent with a stronger growth of water domains, that must accommodate more water, and it can be correlated to swelling of membrane structure [3]. Indeed, it has been adopted a correlation for model parameter ϕ as λ increases, according to Equation 14, to account for a great membrane deformation, calibrated on specific RH steps, i.e. RH 30%, 50%, 70%.

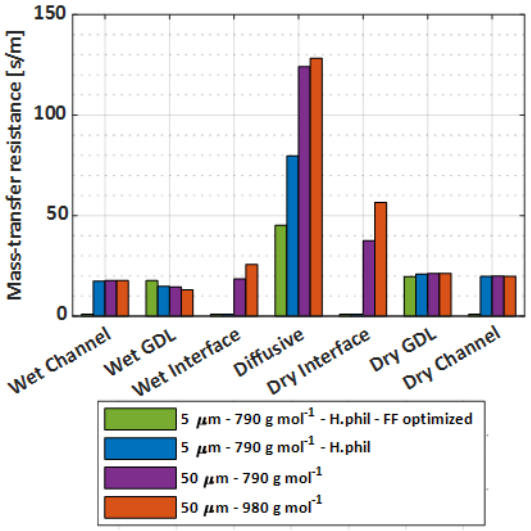

Fig. 3 Individual contribution to water transport trough membrane under several configurations

$$\phi = 0.022(\lambda - 2) + 0.05 \qquad (14)$$

Experimental data have been compared with model simulations also for different temperatures and *EW*, confirming the good adherence between the two.

Once identified PFSA water transport properties, steady state model simulations have been performed at the same operating conditions specified by DOE [12] and reported in Table 1, together with assumption on geometrical dimension of humidifier single cell, to estimate water flux and active membrane area of air humidifier. In Figure 4, individual contributions to mass transport resistance are identified for different membrane and configuration. It can be observed that the main contributions are represented by membrane diffusive resistance and interfacial resistance on dry side. The decrease in *EW* causes a significant reduction in the interfacial resistance on both wet and dry side and a slight decrease in the diffusive one.

Based on the above-mentioned results, it has been observed that counter-flow configuration with such PFSA membranes with *EW* and thickness equal to 790 g mol^{-1} and 5 μm respectively, assembled with hydrophilic porous layer, that lets to minimize membrane interfacial resistances, allows to get an average water flux of 2.3 g m^{-2} s^{-1}, representing 55% of the target proposed by DOE.

It can be observed, from Figure 4, that diffusive resistance is diminished by 38%, after a ten-fold decrease in thickness of membrane, because average membrane water content is very low, in such conditions, causing a strong decrease in water diffusivity. Since channel resistance to mass transport is not negligible, adopting an optimized channel geometry, that lets to strongly reduce its resistance, allows to get an average water flux equal to 3.4 g m^{-2} s^{-1}, in accordance with what has been obtained in [13]. Moreover, it can be seen that reducing gas transport resistance lets to decrease further membrane diffusive resistance. Thus, total water request, equal to 5 g s^{-1}, for a typical automotive stack, can be achieved with a total membrane area of 1.4 m^2. Optimization of operating conditions, as dry air inlet temperature or operating pressure, would allow to further reduce membrane diffusive contribution, increasing average water flux.

5 Conclusions

A water transport model that integrates steady-state vapor permeation and dynamic vapor sorption phenomena through PFSA membranes consistently has been implemented. Thanks to a broad experimental campaign, on low equivalent weight and short-side-chain membranes, water transport properties of such membranes have been determined and model has been calibrated and validated. It has been possible to identify the several contributions to mass transport resistance in a typical humidifier configuration, indicating that mass transfer resistances in the ionomer interfaces and the ionomer layer are of comparable magnitude. By investigating performance for a set of conditions for which air humidifier for automotive fuel cell system should transfer 5 g s^{-1}, model predicts an average value of 3.4 g m^{-2} s^{-1}, that corresponds to a total active area equal to 1.4 m^2.

References

1. D. A. Cullen, K. C. Neyerlin, R. K. Ahluwalia, R. Mukundan, K. L. More, R. L. Borup, A. Z. Weber, D. J. Myers, and A. Kusoglu, Nature Energy **6**, 462 (2021)
2. A. Kusoglu and A. Z. Weber, Chemical Reviews **117**, 987 (2017)
3. A. Kusoglu and A. Z. Weber, in *Polymers for Energy Storage and Delivery: Polyelectrolytes for Batteries and Fuel Cells* (ACS Publications, 2012), pp. 175–199
4. A. Goshtasbi, P. García-Salaberri, J. Chen, K. Talukdar, D. G. Sanchez, and T. Ersal, Journal of The Electrochemical Society **166**, F3154 (2019)
5. M. B. Satterfield and J. B. Benziger, The Journal of Physical Chemistry B **112**, 3693 (2008)
6. N. Zamel and X. Li, Progress in Energy and Combustion Science **39**, 111 (2013)
7. L. M. Pant, M. R. Gerhardt, N. Macauley, R. Mukundan, R. L. Borup, and A. Z. Weber, Electrochimica Acta **326**, (2019)
8. A. Thorell and L. Wadsö, Drying Technology **36**, 332 (2018)
9. A. A. Kulikovsky, Journal of the Electrochemical Society **150**, A1432 (2003)
10. S. Ge, X. Li, B. Yi, and I.-M. Hsing, Journal of The Electrochemical Society **152**, A1149 (2005)
11. K. D. Kreuer, M. Schuster, B. Obliers, O. Diat, U. Traub, A. Fuchs, U. Klock, S. J. Paddison, and J. Maier, Journal of Power Sources **178**, 499 (2008)
12. W. Johnson and W. Gore, *Materials and Modules for Low-Cost, High Performance Fuel Cell Humidifiers* (2012)
13. R. K. Ahluwalia, X. Wang, W. B. Johnson, F. Berg, and D. Kadylak, Journal of Power Sources **291**, 225 (2015)